Multimode Interference Refractive Index Sensor Based on Coreless Fiber

Yang LI[*], Zhibo LIU, and Shuisheng JIAN

Institute of Lightwave Technology, Beijing Jiaotong University, Beijing, 100044, China

[*]Corresponding author: Yang LI   E-mail: 11111025@bjtu.edu.cn

Abstract: A multimode interference refractive index (RI) sensor based on the coreless fiber was numerically and experimentally demonstrated. Two identical single mode fibers (SMF) are spliced at both ends of a section of the coreless fiber which can be considered as the equivalent weakly guiding multimode fiber (MMF) with a step-index profile when the surrounding refractive index (SRI) is lower than that of the coreless fiber. Thus, it becomes the conventional single-mode multimode single-mode (SMS) fiber structure but with a larger core size. The output spectra will shift along with the changes in the SRI owing to the direct exposure of the coreless fiber. The output spectra under different SRIs were numerically studied, as well as the sensitivities with different lengths and diameters of the coreless fiber. The predication and calculation showed the good agreement with the experimental results. The proposed RI sensor proved to be feasible by verification experiments, and the relative error was merely 0.1% which occupied preferable sensing performance and practicability.

Keywords: Refractive index sensor, multimode interference, coreless fiber

1. Introduction

All-fiber refractometer sensors have the significant value and wide application prospects in the biochemical field, and a single-mode multimode single-mode (SMS) fiber structure has attracted great attention recently [1–9] with its distinct advantages of simplicity, ease of fabrication and a variety of functions resulting from the multimode interference effect, providing a new choice for the realization of the all-fiber refractometer. Various techniques have been reported to achieve refractive index (RI) sensing based on the SMS fiber structure. One of these methods is that the multimode fiber (MMF) cladding of an SMS fiber structure is removed and the core is directly exposed to the surrounding medium through the chemical etching technique [10, 11]. As the surrounding refractive index (SRI) changes, the propagation constants for each guided mode within the MMF core will change correspondingly, resulting in shifts in the output spectra. The RI sensing can be achieved through monitoring these shifts. However, to controllably and uniformly remove the cladding, chemical compounds with different concentrations should be applied. This will dramatically increase the fabrication difficulty, and the induced surface roughness may lead to a significant discrepancy between the experimental results and theoretical design. Another all-fiber refractometer based on an

SMS fiber structure was proposed and demonstrated by Q. Wu [12] which is used in combination with a uniform fiber Bragg grating (FBG). The MMF is followed by a fusion splice to the FBG imprinted SMF. The output SMF can be considered as a three-layer structure, and the FBG will reflect both the core mode and cladding modes propagating in it. The reflected wavelength of the core mode remains unchanged while that of selected cladding modes will change as the SRI changes. So the SRI can be determined by monitoring the relative shift between the core mode and cladding modes. The maximum sensitivity achieved by experiments was 7.33 nm/RIU in the RI range from 1.324 to 1.439. This structure preserves the inherent advantages of an SMS fiber structure, but the sensitivity is relatively low by comparison with other all-fiber refractometers. In order to improve the sensitivity, an SMS structure combined with a fiber taper was proposed by P. Wang [13], and an ultrahigh sensitivity, better than 1900 nm/RIU , was achieved within the range of 1.33–1.44. The waist diameter and total length of the MMF taper were $30\,\mu m$ and $675\,\mu m$, respectively. The surrounding changes will get into the core readily, and the propagation constants of the most predominant modes within the MMF are particularly susceptible to the SRI as a result of the enhanced evanescent field in the taper region. Even though the sensitivity is ultrahigh, the easily broken taper section and the complexity of the fabrication process make it unsuitable for practical applications. To preserve the inherent advantages and improve the reliability, an SMS fiber structure based on the coreless fiber is proposed in this paper. A section of the coreless fiber is spliced between two identical SMFs, and the fabrication process is rather simple without introducing other complex techniques. The coreless fiber can be considered as the equivalent MMF with a step-index profile when the SRI is lower than that of the coreless fiber. The output spectra will shift along with the changes in the SRI owing to the direct exposure of the coreless

fiber. In addition, the coreless fiber has the similar outer diameters to the SMFs, which makes such an all-fiber RI sensor unbreakable under the ordinary usage, exhibiting the higher reliability.

2. Principle of operation

The SMS structure based on the coreless fiber, so called the equivalent SMS, is schematically illustrated in Fig. 1(a), and Fig. 1(b) presents the conventional SMS structure for comparison. Two identical single mode fibers are spliced at both ends of a section of the coreless fiber, and the surrounding medium, e.g., solution, can act as its cladding. When the RI of the surrounding medium is lower than that of the coreless fiber and the difference is relatively small, the coreless fiber can be treated as the weakly guiding MMF with a step-index profile. Thus, it becomes the conventional SMS structure but with a larger core size. The incident field from the SMF typically excites higher-order modes together with the fundamental mode of the coreless fiber, consequently, the excited field is a complete set of guided modes. However, if the SMFs and coreless fiber are axially aligned at the splicing points, the power will be coupled only to the first few circularly symmetric modes. And these modes will propagate along the coreless fiber and be subject to the multimode interference effect. At the second splicing point, these circularly symmetric modes will be recoupled to the second SMF. To determine which modes are excited in the coreless fiber and the coupling efficiency, the mode propagation analysis (MPA) [2, 6] successfully used in the conventional SMS is applied to explain the principle of operation.
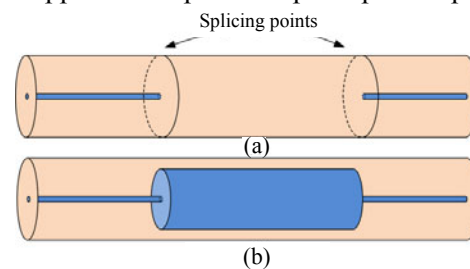

Fig. 1 Two different types of the SMS structures: (a) SMS based on the coreless fiber and (b) conventional SMS.

The transmission loss of an SMS structure is given by [6]

$$P_{\text{out}}(L) = 10 \lg \left(\left| \sum_{n=1}^{N} \eta_n^2 \exp(j\beta_n L) \right|^2 \right) \qquad (1)$$

where L is the length of the MMF, η_n and β_n are the excitation coefficient and propagation constant of LP_{0n} mode, respectively, and N is the total number of guided modes within the coreless fiber. It seems that the transmission loss depends on four parameters from (1). Yet the fact is that all the parameters are directly or indirectly associated with the SRI except for L. The number of guided modes accommodated in an MMF with a step-index profile is determined by its normalized frequency:

$$V = k_0 a_M \sqrt{n_{\text{core}}^2 - n_{\text{clad}}^2} \qquad (2)$$

where a_M, k_0, n_{core}, and n_{clad} are the radius of the MMF, wavenumber in the free space, core and cladding refractive indices, respectively. It is noteworthy that n_{clad} is equal to the SRI for the equivalent SMS which means the SRI and total number of guided modes are closely related. For each specific mode, the propagation constant β_n can be written as

$$\beta_n = k_0 n_{\text{eff}}^{(n)} \qquad (3)$$

where $n_{\text{eff}}^{(n)}$ is the effective RI of LP_{0n} mode which is in connection with the SRI as well. As for the excitation coefficients, they could be calculated by the overlap integral between the input field distribution and field distribution of each guided mode. The field distribution of a specific mode is a function of its propagation constant, and this makes the excitation coefficients indirectly related to the SRI. Consequently, as the SRI varies, both the normalized frequency and propagation constant will change correspondingly, as well as the excitation coefficients. The transmission loss of the proposed RI sensor is merely a function of the SRI at a certain operating wavelength. This is the basic operation principle of such an RI sensor.

3. Simulations and experiments

3.1 Feasibility

To verify the feasibility of the proposed RI sensor, we firstly carried out the numerical simulation by using the MPA. As mentioned above, the SMFs and coreless fiber are perfectly aligned at the splicing points, and the power from the SMF will be coupled only to the first few circularly symmetric modes. That will greatly decrease the total number of guided modes excited by the incident source. However, the number is still considerable owing to the large core size of the equivalent MMF. Therefore, the estimated propagation constant for each specific mode is obviously inaccurate when using the approximate formula described in [14]. In our simulation, we calculated the propagation constants through solving the characteristic equation of LP_{0n} modes instead to ensure the accuracy. The SMFs in our simulation had 4.03-μm and 62.5-μm core and cladding radii, respectively. The coreless fiber is of the same material with the SMF cladding, and the RI is calculated with the Sellmeier formula. The relative RI difference of the SMF was 0.36%.

The transmission loss of the proposed RI sensor is a function of the SRI at a certain operating wavelength as described in Section 2. Under such conditions, we set the other parameters at fixed values and then simply changed the SRI to prove this. The computed results are presented in Fig. 2, and the outer diameter and length of the coreless fiber are $104\,\mu\text{m}$ and $4.12\,\text{cm}$, respectively. We can clearly see that the output spectra exhibit blue spectral shifts with increasing the SRI ranging from 1.333 to 1.4. Besides, there are more than one minimum point in the output spectrum, namely the characteristic wavelength or dip wavelength. RI sensing can be achieved through the shifts measurement of these characteristic wavelengths. The inset of Fig. 2 shows the simulated and experimental spectral responses of the equivalent

SMS fiber structure when the length of the coreless fiber and SRI were 4.12 cm and 1, respectively.
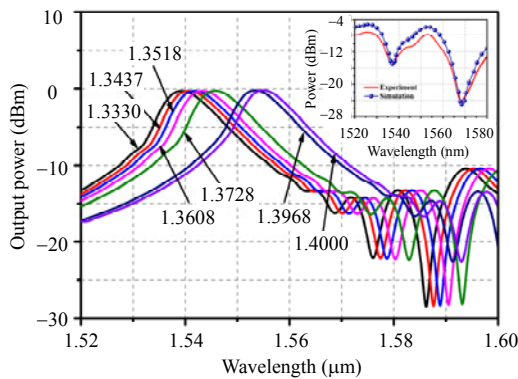

Fig. 2 Output responses with different SRIs: the outer diameter and length of the coreless fiber are 104 μm and 4.12 cm [the inset is the comparison between the simulated and experimental spectral responses (SRI=1)].

3.2 Influence of the length

And then we investigated the influence of the coreless fiber length on the sensitivity of such a refractometer. It is generally appreciated that, for RI sensing, the larger overlap between the propagating mode and surrounding medium tends to have a higher sensitivity. Therefore, the sensitivity mainly depends on the degree of impact on the mode effective refractive index. However, we can see that the length of the coreless fiber has nothing to do with the mode effective refractive index from (3). In such a case, the sensitivity should remain unchanged regarding the variations in the coreless fiber length.

The length of the coreless fiber varied from 3.98 cm to 5.71 cm, while the outer diameter was constant in numerical simulations. We measured the characteristic wavelengths under different SRIs with variable L, and the results are deposited in Fig. 3. The characteristic wavelength will blue shift as the SRI increases from Fig. 3. On the other hand, the most pronounced and important feature in the graph is that the proposed refractometer's sensitivity, slope of the curves, remains unchanged as the length varies. The only difference is the intercept resulting from the measurements of the characteristic wavelength at different positions. This result is in
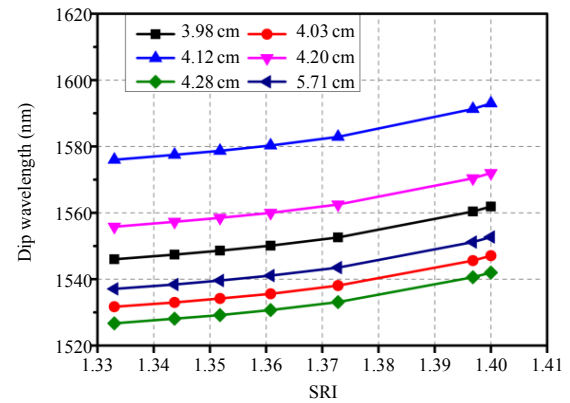
consistent with our previous analysis.

Fig. 3 Outer diameter of the coreless fiber is 104 μm, dip wavelength shifts with different L.

The configuration shown in Fig. 4 is constructed to test and verify our simulation results. The solution used in our experiments was the Glycerin solution with different concentrations. The SRI ranged from 1.333 to 1.3968 in the room temperature.
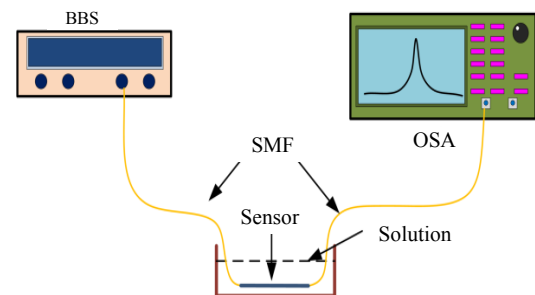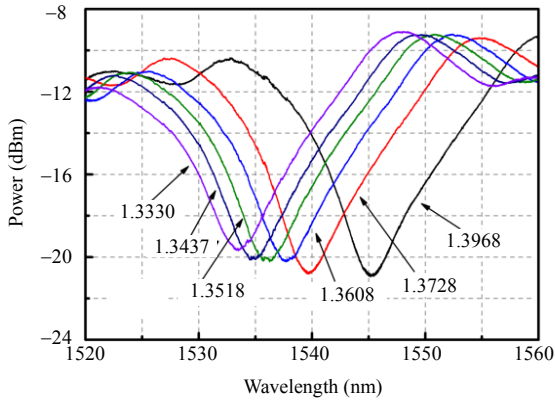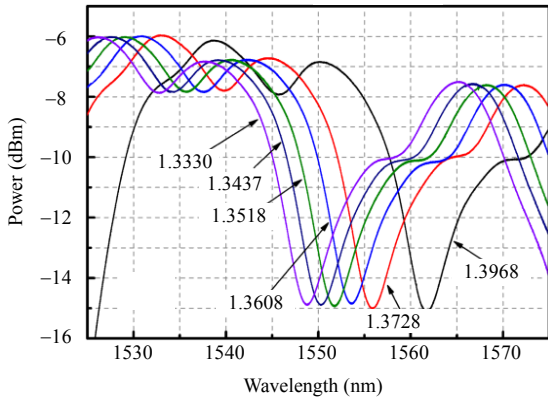

Fig. 4 Experimental setup (BBS: broad band source; OSA: optical spectrum analyzer).

It has been demonstrated that the length of the coreless fiber has no effect on the sensor's sensitivity, so three random lengths of the coreless fiber, in the vicinity of the self-imaging distance, have been chosen to make three sensors in practical experiments. The coreless fiber was made by our laboratory through drawing the tower, and the outer diameter was 104 μm. The RI of such a fiber can be calculated by the Sellmeier equation according to its dispersion property. The output spectra under different SRIs are presented in Fig. 5. From Fig. 5, we can see that as the SRI increases, the characteristic wavelengths will blue shift which is the same as the simulation results. Besides, there are
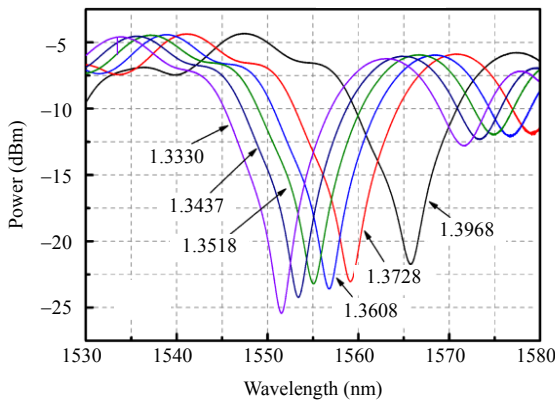
more than one characteristic wavelength in the spectra which is in consistent with the simulation results as well. The measured wavelength shifts are shown in Fig. 6. The calculated and measured results are in reasonable agreement by comparison between Figs. 3 and 6.
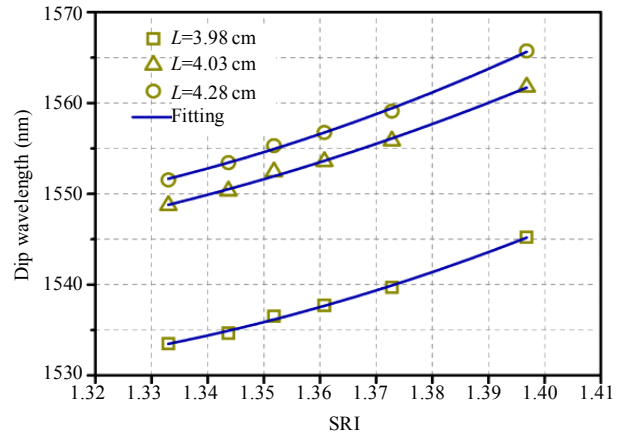

Fig. 6 Dip wavelength shift vs. SRI.

3.3 Influence of the diameter

The total number of excited modes is mainly decided by the core radius from (2), and it will decrease as the diameter decreases. The propagation constants of the predominant modes within the coreless fiber trend to be greatly affected by a small change in the SRI in such conditions. For proofing

(a)

(b)

(c)

Fig. 5 Output spectra under different SRIs: (a) *L*=3.98 cm, (b) *L*=4.03 cm, and (c) *L*=4.28 cm.
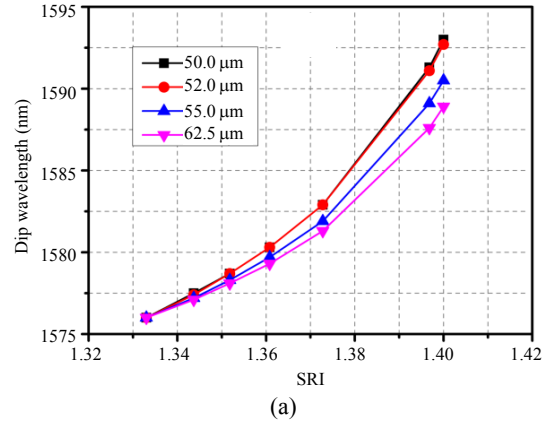
(a)
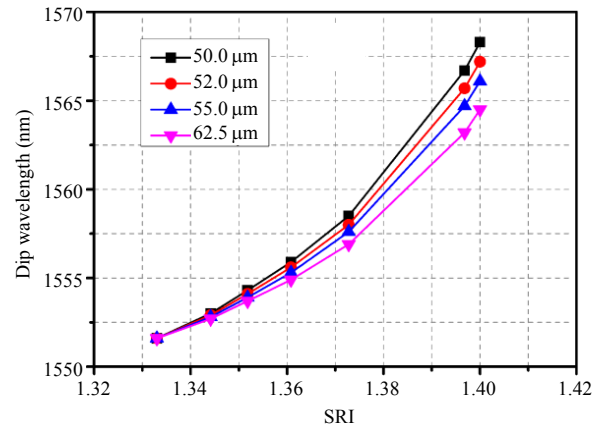
(b)

Fig. 7 Sensitivities of different coreless fiber radii: (a) *L*=4.12 cm and (b) *L*=4.20 cm.

this point, we set the length of the coreless fiber at a fixed value and investigated the influence of the outer diameter on the sensitivity. The outer diameter of the coreless fiber ranged from $100\,\mu m$ to $125\,\mu m$. The simulation results are shown in Fig. 7. The length of the coreless fiber in Fig. 7(a) was 4.12 cm while that in Fig. 7(b) was 4.20 cm. For the sake of clarity, the plots have been shifted vertically. It is obvious that the smaller radius is, the higher sensitivity is. This cannot be verified by the experiment because there is no other fiber diameter available at present. However, this result is completely credible.

4. Confirmatory experiments

In order to further test the sensing performance and evaluate the practicability of this sensor, we carried out a confirmatory experiment. We used the 4.0-cm-length RI sensor to measure the RI of absolute ethyl alcohol in the room temperature. It is known that the RI of absolute ethyl alcohol in the room temperature is 1.3612. We conducted a total of eight measurements, and two of the output spectra are shown in Fig. 8. There are two dips in the output spectrum, and Dip 2 is corresponding to the middle curve in Fig. 6. The average measured RI of absolute ethyl alcohol in the room temperature is 1.3598, and the relative error was 0.1%. Figure 9 presents the relative errors of each measurement. The confirmatory experiments' results reveal that the proposed RI sensor possesses the excellent
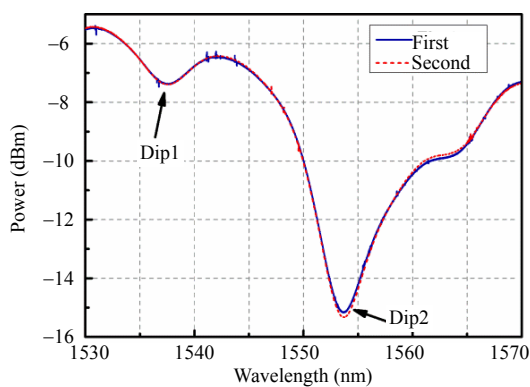

Fig. 8 Output spectra of the RI sensor in two measurements.

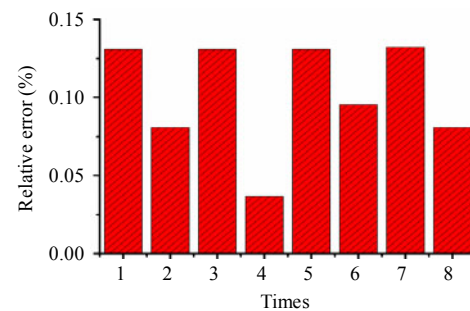measurement repeatability and potential for the practicability.

Fig. 9 Relative error of the eight measurements.

5. Conclusions

We have numerically and experimentally demonstrated a multimode interference RI sensor based on the coreless fiber. Under the weakly guiding condition, the spectral responses were simulated by using the MPA method. Numerical simulations indicate that the characteristic wavelength in the output spectra will shift as the SRI changes. And we have proved that the length of the coreless fiber has no influence on the sensitivity both by simulations and experiments. The comparison between the calculated and measured results shows that they are in reasonable agreement. The impact of the diameter of the coreless fiber on the sensitivity was numerically studied as well, and the results show that a smaller diameter tends to have a higher sensitivity. In the confirmatory experiments, a relative error, merely 0.1%, has been successfully achieved by a coreless fiber with an outer diameter of $104\,\mu m$ and a length of 4.0 cm. This equivalent SMS preserves the inherent advantages of an SMS fiber structure and exhibits the higher reliability and preferable practicability.

References

[1] D. Đonlagi and M. Završnik, "Fiber-optic microbend sensor structure," *Optics Letters*, 1997, 22(11): 837–839.

[2] W. S. Mohammed, A. Mehta, and E. G. Johnson, "Wavelength tunable fiber lens based on multimode interference," *Journal of Lightwave Technology*, 2004, 22(2): 469–477.

[3] Z. Huang, Y. Zhu, X. Chen, and A. Wang, "Intrinsic Fabry-Pérot fiber sensor for temperature and strain measurements," *IEEE Photonics Technology Letters*, 2005, 17(11): 2403–2405.

[4] E. Li, X. Lin, and C. Zhang, "Fiber-optic temperature sensor based on interference of selective higher-order modes," *Applied Physics Letters*, 2006, 89(9): 091119-1–091119-3.

[5] E. Li, "Sensitivity-enhanced fiber-optic strain sensor based on interference of higher order modes in circular fibers," *IEEE Photonics Technology Letters*, 2007, 19(10): 1266–1268.

[6] Q, Wang, G. Farrell, and W. Yan, "Investigationon single-mode-multimode-single-mode fiber structure," *Journal of Lightwave Technology*, 2008, 26(5): 512–519.

[7] S. M. Tripathi, A. Kumar, R. K. Varshney, Y. B. P. Kumar, E. Marin, and J. P. Meunier, "Strain and temperature sensing characteristics of single-mode-multimode-single-mode structure," *Journal of Lightwave Technology*, 2009, 27(13): 2348–2356.

[8] K. Wang, D. Klimov, and Z. Kolber, "Seawater pH sensor based on the long period grating in a single-mode-multimode-single-mode structure," *Optical Engineering*, 2009, 48(3): 034401.

[9] Q. Wu, Y. Ma, J. Yuan, Y. Semenova, P. Wang, C. Yu, *et al.*, "Evanescent field coupling between two parallel close contact SMS fiber structures," *Optics Express*, 2012, 20(3): 3098–3109.

[10] Q. Wang and G. Farrell, "All-fiber multimode-interference-based refractometer sensor: proposal and design," *Optics Letters*, 2006, 31(3): 317–319.

[11] Q. Wu, Y. Semenova, P. Wang, and G. Farrell, "High sensitivity SMS fiber structure based refractometer-analysis and experiment," *Optics Express*, 2011, 19(9): 7937–7944.

[12] Q. Wu, Y. Semenova, B. Yan, Y. Ma, P. Wang, C. Yu, *et al.*, "Fiber refractometer based on a fiber Bragg grating and single-modemultimode single-mode fiber structure," *Optics Letters*, 2011, 36(12): 2197–2199.

[13] P. Wang, G. Brambilla, M. Ding, Y. Semenova, Q. Wu, and G. Farrell, "High-sensitivity, evanescent field refractometric sensor based on a tapered, multimode fiber interference," *Optics Letters*, 2011, 36(12): 2233–2235.

[14] D. Marcuse, "Mode conversion in optical fibers with monotonically increasing core radius," *Journal of Lightwave Technology*, 1987, 5(1), 125–133.